





 Cite this: *J. Anal. At. Spectrom.*, 2024, **39**, 2409

Determining the sources of (sub)permil-level inaccuracy during laser ablation-MC-ICPMS boron isotope measurements of carbonates†

 Douglas Coenen,  *^{ab} David Evans,  ‡^{ab} Hana Jurikova,^c Matthew Dumont,^c James Rae  ^c and Wolfgang Müller^{ab}

Recent developments in spatially-resolved boron isotopic analysis using laser ablation as a means of sample introduction to MC-ICPMS instruments (LA-MC-ICPMS) increasingly allow researchers to explore the spatial heterogeneity of the boron isotopic composition of a range of geochemical applications, for example in palaeoclimatology and mantle petrology. However, previous work has shown that a diffuse interference centred near ^{10}B , when measuring samples with a calcium-rich matrix, can significantly bias especially the measurement on ^{10}B , affecting the accuracy of boron isotope measurements. Although several correction approaches have yielded sufficiently accurate analyses of $\delta^{11}\text{B}$ in calcium carbonate, the root cause of this interference is still not fully resolved. Here, we explore the various potential sources of inaccuracy in boron isotope measurements made using (LA-)MC-ICPMS by experimenting with dry and wet plasma conditions, in both solution and laser ablation mode (in the former case, our solution (Ca–Mg)/B ratios broadly mimic those found in natural samples). In solution mode, we find that irrespective of wet or dry plasma conditions, the introduction of a Ca-containing matrix yields a baseline up to ~ 4 and ~ 14 times higher around $m/z \approx 10$ for wet and dry plasma conditions, respectively, compared to both a Mg-only matrix and lack of matrix. In order to explore this further, we performed mass scans around $m/z \approx 10$ during laser ablation of different carbonates with varying matrix [Ca]. These show that the $m/z \approx 10$ interference scales linearly with a mixture of the calcium content of the analyte matrix and $^{40}\text{Ar}^{4+}$ ion beam intensity, as previously hypothesised. Moreover, by experimenting with different plasma loading scenarios during the ablation of CaCO_3 , *i.e.* varying laser spot sizes, we find that permil-level inaccuracies in $\delta^{11}\text{B}$ may occur when the analyte ablated mass is significantly different than that of the standard used to calibrate instrumental mass bias. This is important given that we also show that different commonly-used reference materials ablate at very different rates, which illustrates the need for a careful standardisation approach irrespective of broader matrix effects when sub-permil level accuracy and precision are desirable when utilising LA-MC-ICPMS.

 Received 23rd April 2024
 Accepted 23rd July 2024

DOI: 10.1039/d4ja00154k

rsc.li/jaas

Introduction

The precise and accurate measurement of the boron isotopic composition of geological materials has become increasingly useful in various branches of geochemistry (for a review see Marschall and Foster, 2018).¹ Boron isotopes serve as a valuable tracer and provide insights into processes in the fields of

igneous and metamorphic petrology,^{2,3} past variations of pH/ CO_2 ,⁴ and biomineralisation.^{5,6}

The analysis of biogenic carbonate samples to study calcification and past seawater pH is performed most precisely using thermal ionisation mass spectrometry (TIMS) and multi-collector induced coupled plasma mass spectrometry (MC-ICPMS) after chemical purification.^{7–9} These methods are well suited for the precise analysis of boron isotopic composition (0.1–0.3‰, 2 SD for P-TIMS¹⁰ and 0.2–0.3‰, 2 SD for MC-ICPMS⁷ of bulk biogenic carbonate samples), and usually require sample sizes containing ng levels of boron (between 20 ng and 100 ng for P-TIMS¹⁰ and between 2.5 ng and 20 ng for MC-ICPMS).^{7,11} These methods, however, cannot provide the spatial resolution needed for revealing the heterogeneity of boron isotopic composition in certain samples. Secondary Ion Mass Spectrometry (SIMS) has been used to assess internal heterogeneities in various materials including carbonates,^{12,13}

^aInstitute of Geosciences, Goethe University Frankfurt, Frankfurt am Main, Germany.
 E-mail: Coenen@geo.uni-frankfurt.de

^bFrankfurt Isotope and Element Research Center (FIERCE)Goethe University Frankfurt, Frankfurt am Main, Germany

^cSchool of Earth and Environmental Sciences, University of St Andrews, St Andrews, UK

† Electronic supplementary information (ESI) available. See DOI: <https://doi.org/10.1039/d4ja00154k>

‡ Now at: School of Ocean and Earth Science, University of Southampton, Southampton, UK.



however, the costly and time consuming nature of these measurements coupled with the lack of suitable, well-characterised reference materials, limits the accessibility of this technique for highly spatially-resolved boron isotope analysis in calcium carbonate samples and is one reason that the precision of this technique is typically worse ($\sim 0.6\text{--}1\%$, SD).

The development of laser ablation as a sample introduction technique for MC-ICPMS has gained traction for the boron isotopic measurements of geological materials over the past two decades.^{14,15} However, the accurate determination of the boron isotopic composition of calcium carbonate samples using laser ablation (LA)-MC-ICPMS is not without challenges. Indeed, recent work has shown that the widely used Neptune Plus (Thermo Fisher Scientific) MC-ICPMS is characterised by a diffuse interference in the m/z range between 10 and 11 when ablating samples with calcium-rich matrices.^{16–20} Several methodologies have been developed to accurately correct for this *via* the use of a suite of inter-laboratory calibrated standards, since typical background correction cannot account for this matrix specific baseline elevation.^{17–19} This interference has been attributed to scattered Ca ions in the flight tube and is not limited to calcium carbonate, but also other calcium-rich matrices.¹⁹ In contrast, previous work with alternative MC-ICPMS instrumentation such as the Plasma II (Nu instruments)^{21,22} and the AXIOM (Thermo-Fisher Scientific)^{23,24} were seemingly not characterised by a Ca-derived boron isotope measurement inaccuracy when ablating calcium carbonate samples. This has been attributed to either differences in the MC-ICPMS instrumentation or the use of femto-second rather than nano-second laser ablation instruments,^{21,22} although more recent work²⁰ has shown that the interference around $m/z \approx 10$ was also present during laser ablation measurement of calcium carbonate samples in the Plasma II and AXIOM when the measurements were performed using Faraday cups, in contrast to the majority of previous studies utilising ion counters. Indeed, this relationship with the choice of instrument detector corroborates previous findings,¹⁸ suggesting that matrix effects depend more on the type of detectors (and any pre-detector deflection or filtration) than the choice of instrument, given that the previous reports of a lack of $m/z \approx 10$ interference used the ion counters with deflectors.^{21–24} While this might imply that future studies should “simply” use ion counters, the use of Faraday cups, especially when connected to $10^{13} \Omega$ amplifiers, is desirable from an accuracy and precision point of view when the B concentration of the sample allows it.²⁵

While enormous progress has been made in our understanding of the major source of inaccuracy in LA-MC-ICPMS analysis of Ca-rich samples, this progress and the coincident improvement in data quality serve to highlight that other sources of inaccuracy exist when making these measurements. Indeed, previous work has shown that LA-MC-ICPMS analysis is associated with matrix effects independent of the sample [Ca] depending on instrument tuning¹⁹ and can suffer from the effects of plasma mass loading,^{26,27} with both factors potentially resulting in boron isotope inaccuracies of up to several permil. This latter bias appears to be present regardless of the detector

and is thus associated with ionisation behaviour in the plasma.^{17,26,27}

This contribution explores the different sources of inaccuracy in boron isotopic measurement using a laser ablation system coupled to a Neptune plus MC-ICPMS with Faraday cups, *via* (1) systematic experiments ablating Mg- or Ca-rich matrices and (2) plasma loading. For comparison, we perform solution measurements using solutions with Ca and Mg matrices with constant [B] with (Ca-Mg)/B ratios broadly mimicking those found in natural samples.

Materials and methods

All boron isotopic measurements were performed using a Neptune Plus MC-ICPMS, operated in both laser-ablation and solution modes, at the Frankfurt Isotope and Element Research Center (FIERCE), Goethe University Frankfurt.

Laser ablation MC-ICPMS setup

The spatially-resolved boron isotopic measurements overall followed the methodology of Evans *et al.* (2021).¹⁹ A RESolution LR 193 nm ArF LA system (Applied Spectra, formerly Resonetics) was connected to a Neptune Plus MC-ICPMS (Thermo Fisher Scientific) *via* nylon-6 tubing.²⁸ The RESolution LR is equipped with the large Laurin Technic S-155 two-volume ablation cell and He was used as the main cell gas, with Ar sample gas from the MC-ICPMS admixed into the top of the inner cell funnel. N₂ was added downstream of the ablation cell to improve sensitivity.²⁹ Solution-MC-ICPMS experiments utilized the same mass spectrometer, with both an Aridus desolvator and a “standard” glass spray chamber used as sample introduction systems to achieve dry and wet solution plasma conditions, respectively (detailed below). Typical tuning used for the laser ablation and solution MC-ICPMS analysis is detailed in Table 1.

The Faraday cups were arranged to simultaneously measure ¹⁰B (L4) and ¹¹B (H4), as well as $m/z \approx 10.035$ (L3) and $m/z \approx 9.979$ (L5) to monitor the Ca interference that is present across the mass range 10–11 on the Neptune.^{17–19} All measurements were performed at low mass resolution, with $10^{13} \Omega$ resistors installed on all four cups. Tuning in LA mode was performed by ablating NIST SRM 612 with a 90 μm circular spot at 6 Hz repetition rate and $\sim 6 \text{ J cm}^{-2}$ fluence to achieve a sensitivity between 1.5–3.1 mV per $\mu\text{g g}^{-1}$ and a background measurement on ¹¹B between 0.3 to 2 mV, corresponding to a useful ion yield (counted/ablated) in LA mode between 1.5×10^{-4} and 2.9×10^{-4} .

In order to determine/corroborate the source of the matrix-induced interference, primarily on ¹⁰B,^{17–19} a suite of well-characterised calcium carbonate standards were used to establish the empirical relationship between the measured $\delta^{11}\text{B}$ inaccuracy (the difference between the measured $\delta^{11}\text{B}$ and the solution-derived reference/information value of the standard; denoted $\Delta\delta^{11}\text{B}$) and the boron concentration of the sample. The three pressed powder pellet carbonate reference materials used for this purpose include JcP-1 (*Porites* sp.), JcT-1 (*Tridacna*



Table 1 Solution and LA-MC-ICPMS ablation and tuning parameters utilised here

MC-ICPMS: Neptune plus	
Cup configuration	L5: 9.979, L4: ^{10}B , L3: 10.035, C: 10.56, H4: ^{11}B
Amplifiers	$10^{13} \Omega$ on all cups except C (10^{11})
Sample/skimmer cone	Ni Jet/X
Laser: dry plasma	
RF power	1280–1380 W
Ar sample gas	1.005–1.300 L min $^{-1}$
Laser: wet plasma	
RF power	1347 W
Ar sample gas	0.600 L min $^{-1}$
Ar add gas (to spray chamber)	0.400 L min $^{-1}$
Solution: dry plasma (Aridus)	
RF power	1350 W
Ar sample gas	0.800 L min $^{-1}$
Ar sweep gas	6.10 L min $^{-1}$
N $_2$ gas	2 mL min $^{-1}$
Nebuliser	100 μL min $^{-1}$
Solution: wet plasma (spray chamber)	
RF power	1325 W
Ar sample gas	1.135 L min $^{-1}$
Nebuliser	100 μL min $^{-1}$
RESolution LR (S-155 cell)	
Beam diameter	33–285 μm
Repetition rate	6 Hz
Fluence	2–10 J cm $^{-2}$, typically 6 J cm $^{-2}$
He gas flow	300–400 mL min $^{-1}$
N $_2$ gas flow	3.0–7.5 mL min $^{-1}$
Typical tuning parameters	
ThO $^+$ /Th $^+$	5–35%
U $^+$ /Th $^+$	1.3–1.8
$^{44}\text{Ca}^{2+}/^{44}\text{Ca}^+$	2–5%
NaI 30	0.20–0.31
Sensitivity	2–4 mV per $\mu\text{g g}^{-1}$ (NIST SRM 612, 90 μm)
Useful ion yield	1.3×10^{-4} – 2.9×10^{-4}
^{11}B background (fully tuned)	0.5 to 3 mV

gigas), both prepared by Edmund Hathorne (GEOMAR) with a $\delta^{11}\text{B}$ value measured by solution MC-ICPMS of $24.36\text{‰} \pm 0.45\text{‰}$ and $16.39\text{‰} \pm 0.60\text{‰}$ respectively (2 SD of interlaboratory averages),³¹ and MACS-3 (USGS synthetic calcite)³² with a $\delta^{11}\text{B}$ solution value of $-1.22\text{‰} \pm 0.20\text{‰}$ (2 SD).³³

To assess the reproducibility and accuracy of the LA-MC-ICPMS measurements, two calcite standards from natural marbles (UWC-1 and UWC-3)³⁴ as well as an in-house inorganic calcite standard (DE-B) were used. UWC-1 was determined by Standish *et al.* (2019)¹⁸ to have $\delta^{11}\text{B} = 7.77\text{‰} \pm 0.89\text{‰}$ (2 SD of 3 replicates) using solution MC-ICPMS. UWC-3 and DE-B were recently characterised by solution MC-ICPMS,³³ yielding $\delta^{11}\text{B} = 20.25\text{‰} \pm 0.08\text{‰}$ (2 SD of 2 replicates) and $-0.02\text{‰} \pm 0.41\text{‰}$ (2 SD of 20 replicates) respectively. Using these three calcium carbonate standards we can assess the intermediate precision (also termed within-lab external reproducibility) of the

methodology over ~ 40 sessions spanning the last 4 years. The intermediate precision of these three standards is as follows: UWC-3: 1.52‰ (2 SD of the 40 session averages), UWC-1: 1.80‰ , and DE-B: 0.95‰ .³³

Solution/laser MC-ICPMS setup

Wet plasma with nebulizer. In order to achieve a wet plasma during laser ablation, we attached a spray chamber with a 100 $\mu\text{L min}^{-1}$ Milli-Q water (18.2 M Ω cm) flow, in addition to the tubing from the laser ablation cell. The additional gas line from the Neptune-plus MC-ICPMS was connected to the spray chamber so that the Ar flow was divided between the laser ablation cell and the spray chamber (for aspiration). The wet aerosol (Milli-Q water) was mixed with the dry aerosol from the laser ablation cell just before the plasma torch with a two-way connector. The laser ablation cell sample gas was 0.6 L min $^{-1}$ while the add gas line connected to the spray chamber had an argon flow of 0.4 L min $^{-1}$. Solution mode MC-ICPMS mass scans were performed in the range $m/z \approx 9.9$ to $m/z \approx 11.1$. The wet plasma was tuned in a similar manner to the dry plasma sessions described above by optimising boron signal intensity over plasma robustness. Tuning parameters can be found in Table 1.

To explore the potential rise in background voltage around ^{10}B , as seen in a dry plasma, six solutions with 25 ng mL $^{-1}$ of boron and varying Ca and Mg concentrations were analysed, bracketed by a blank HNO $_3$ solution (5%). These solutions were prepared by mixing Ca, Mg (both with a concentration of 10 mg mL $^{-1}$ in 5% HNO $_3$, from Thermo Fisher, 99.999% pure), and B ICP standard solutions (1000 ng mL $^{-1}$ from Thermo Fisher). An HNO $_3$ solution (5%) with a boron concentration of 25 ng mL $^{-1}$ was used to tune the instrument. Three sets of concentrations for both Ca and Mg were used, 103 mg L $^{-1}$, 206 mg L $^{-1}$, and 309 mg L $^{-1}$, resulting in (Ca–Mg)/B ratios of 4120, 8240, and 12 360 respectively, which span a range of B/(Mg + Ca) between 300 and 900 $\mu\text{mol mol}^{-1}$ which are typical of a range of natural carbonate samples.

Dry plasma with Aridus. To mimic dry plasma conditions during solution MC-ICPMS analysis, an Aridus II desolvation system (CETAC Technologies Omaha) was used. The instrument was tuned for maximum sensitivity, similarly to the measurements made in laser ablation mode (see Table 1 for ICPMS parameters). The Aridus Ar sweep gas was 6.10 L min $^{-1}$ and the N $_2$ flow was 2 mL min $^{-1}$ (see Table 1). The same B/(Mg + Ca) solutions described above were analysed with an uptake rate of 100 $\mu\text{L min}^{-1}$.

Ablation rate measurement. Ablation crater morphologies were determined using a Keyence digital microscope (model VHX-7000), following a fluence calibration (using a Coherent energy probe) of the laser ablation system. Most samples were analysed at 6 J cm $^{-2}$, but samples from each category, namely solid, pressed-pellet, and nano-pellet, were used to test the relationship between fluences and ablation rates at two further fluences (2 J cm $^{-2}$ and 10 J cm $^{-2}$). Each material was ablated 15 times for 60 s at 6 Hz at a given fluence, with the values we report based on the mean of these individual analyses.



The depth of an ablated crater was calculated by measuring the difference in height of the stage (resolution of 0.1 μm) between the bottom and top of the ablation pit. Using this measurement, the ablation rate of the material was calculated by dividing the measured depth by the number of laser pulses made during the analysis. Laser ablation craters invariably narrow as depth increases, with the characteristics of the variation with depth depending on the details of the optics of the beam delivery system used (*e.g.* working distance, focal length, depth of focus).^{35–37} Therefore, the volume of the ablated crater was calculated by assuming a conical frustum geometry defined as follows:

$$V = \frac{1}{3}\pi h(R_1^2 + R_1R_2 + R_2^2) \quad (1)$$

where h is the crater depth, R_1 is the radius at the top of the crater and R_2 is the radius at the bottom of the crater. Measuring the geometry of the bottom of the crater was associated with some uncertainty, especially in highly reflective materials, such that we assumed that R_2 was 10% lower than R_1 for the number of laser pulses and laser beam diameter utilised here, which was the case for the few ablation craters where it was possible to measure R_2 precisely.

Results and discussion

Exploring the sources of boron isotope inaccuracy

Solution experiments with matrix elements. Unlike laser ablation measurements, solution measurements of boron isotopes usually involve chemical purification to isolate boron from its matrix to prevent any potential matrix interference.³⁸ To determine the possible presence of the background elevation around $m/z \approx 10$, we report results of detailed mass scans around $m/z \approx 10$ for solutions with the same [B], but different Ca/Mg matrix concentrations ranging from no matrix to $\sim 300 \text{ mg L}^{-1}$, under wet (using a spray chamber) and dry plasma conditions (using a desolvator; Fig. 1).

During analysis of a B solution in a Ca matrix, for both dry and wet plasma conditions, the previously reported background elevation around $m/z \approx 10$ during laser ablation of carbonates^{17–19} is present and is between ~ 4 to ~ 14 times more elevated than the matrix-free boron solution (Fig. 1). Mass scans around $m/z \approx 10$ made during wet plasma analysis (using a spray chamber) show that the interference remains in a similar range of 370–500 μV (as does the $^{40}\text{Ar}^{4+}$ ion beam intensity, between 62–83 mV) when increasing the Ca matrix concentration. In the wet plasma, the B sensitivity scales positively with the Ca matrix concentration, with B sensitivity increasing from 1.3 mV per $\mu\text{g g}^{-1}$ at 100 mg L^{-1} Ca matrix to 8.1 mV per $\mu\text{g g}^{-1}$ at 300 mg L^{-1} , although we note that the lower [Ca] matrix has a sensitivity below that of the matrix-free solution (3.8 mV per $\mu\text{g g}^{-1}$). During the analysis in dry plasma conditions however, the sensitivity remains around $0.24 \pm 0.03 \text{ mV per } \mu\text{g g}^{-1}$ (2 SD of the boron sensitivity of the three Ca matrix solutions) among the three Ca matrix solutions, while the interferences and $^{40}\text{Ar}^{4+}$ peak varies with the matrix concentration. For dry plasma conditions, the interference

scales negatively with the Ca matrix concentration, from 690 to 205 μV for the low and high [Ca] solutions respectively (Fig. 1a). This is potentially due to the reduced sensitivity of the plasma when adding a substantial matrix, as potentially evidenced by the fact that the $^{40}\text{Ar}^{4+}$ ion beam intensity scales (decreases) in a similar manner with the matrix [Ca], decreasing from 5.4 to 1.63 mV. In addition, we stress that matrix concentrations such as these would not normally be introduced into a desolvating nebuliser system, and the above results should be viewed within the context of this experimental approach; for example, it may be that the membrane becomes partially clogged at these very high matrix concentrations (up to 300 mg L^{-1}).

In the analyses of B solutions in a variable [Mg] matrix, the background elevation around $m/z \approx 10$ appears to be essentially absent given the interference is within the range of the matrix-free solution measurement in both wet and dry plasma conditions (Fig. 1b and d), demonstrating that the matrix effects observed in laser ablation studies^{17–19} are unlikely to result from other matrix elements. Under dry plasma conditions, the boron sensitivity of the high-matrix solution is higher than the matrix-free solution and the sensitivity decreases with increasing matrix concentration, from 2.7 mV per $\mu\text{g g}^{-1}$ at 100 mg L^{-1} Mg to 1.5 mV per $\mu\text{g g}^{-1}$ at 300 mg L^{-1} , relative to the matrix-free boron solution with a sensitivity of 1.15 mV per $\mu\text{g g}^{-1}$. Under wet plasma conditions, the boron sensitivity of the solution containing a Mg matrix is also higher than the matrix-free solution: the boron sensitivity is on average $10.45 \pm 1.20 \text{ mV per } \mu\text{g g}^{-1}$ (2 SD of the three solutions) across the three Mg matrix solutions. No discernible trend between boron sensitivity and Mg matrix concentration is found during the solution analysis with a spray chamber (Fig. 1d). This broadly contrasting behaviour of analyte (boron) sensitivity between Ca- or Mg-bearing solutions, where a Ca matrix reduces sensitivity while a Mg matrix results in an increase, has been previously reported in Pb isotope studies.³⁹

Fietzke and Anagnostou (2023)²⁰ suggested that in addition to scattered Ca ions, scattered Ar^+ ions contribute to the broad baseline around $m/z \approx 10$. This would explain the background elevation around the $^{40}\text{Ar}^{4+}$ and $^{10}\text{B}^+$ ion beam during blank measurements observed in mass scans, as well as our observation that the broad baseline interference scales with the $^{40}\text{Ar}^{4+}$ peak for the Ca matrix solution analysis under dry and wet plasma conditions (Fig. 1a and c). However, our Mg-matrix data diverge from this interpretation: under dry plasma conditions the $^{40}\text{Ar}^{4+}$ ion beam scales negatively with the Mg matrix concentration while the background elevation around $m/z \approx 10$ remains within the range of the matrix-free measurement (Fig. 1b). However, this may be because the $^{40}\text{Ar}^{4+}$ signal of the Mg solution analysis under dry plasma conditions are comparatively low, from 3.6 to 1.1 mV for low and high [Mg] solutions respectively.

Overall, these experiments conclusively demonstrate that the interference around $m/z \approx 10$ is also present during solution analysis when a Ca matrix is present, under both dry and wet plasma conditions, while (i) the presence of a Mg matrix does not result in any resolvable background elevation and (ii) there



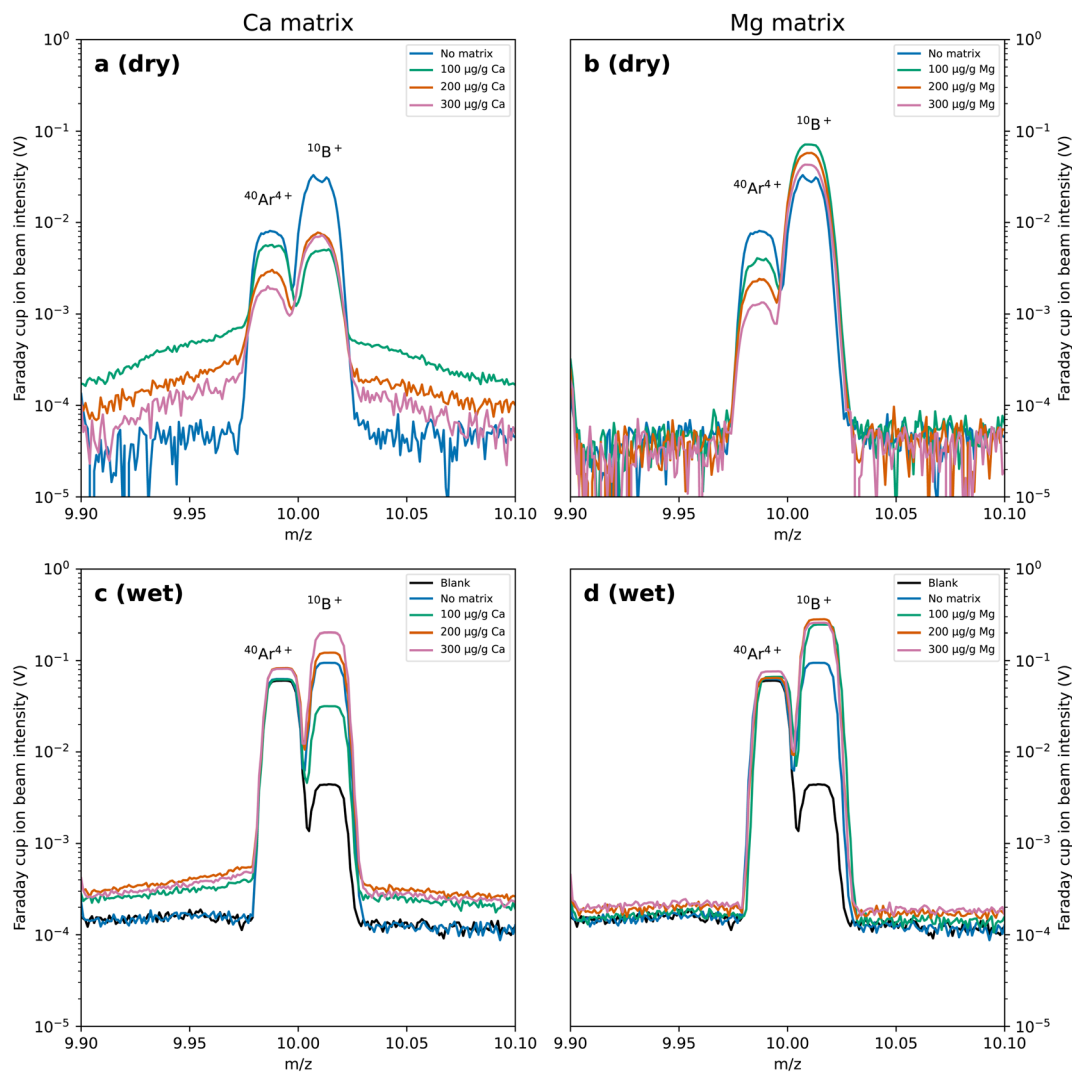


Fig. 1 Mass scans across the m/z range from 9.90 to 10.10 under both dry and wet plasma conditions on a Neptune Plus in solution mode. The Faraday cup ion beam intensity is given as the $10^{11} \Omega$ equivalent on a logarithmic scale. All solutions had a boron concentration of $25 \mu\text{g L}^{-1}$, with three spiked with a substantial Ca or Mg matrix (see Methods). (a) Displays the mass scans of the solution with a Ca matrix and (b) with a Mg matrix, both were measured using a Aridus desolvator to mimic dry plasma conditions. (c) and (d) show measurements of the same solutions as (a) and (b) under wet plasma conditions (sample introduction via a glass spray chamber). A blank solution ($5\% \text{HNO}_3$) was also analysed under wet plasma conditions, displayed in black in (c) and (d).

is no clear link between the $^{40}\text{Ar}^{4+}$ ion beam and the degree of baseline elevation, thus confirming that Ca is the main cause.

The impact of a wet plasma on LA boron isotope data. To the best of our knowledge, no experiments aspirating water downstream of the laser ablation system while measuring boron isotopes by LA-MC-ICPMS have been published, hence the exploration presented here which was initially performed as a potential method of reducing matrix-induced effects (as has been suggested in the case of other isotope systems).^{40–42}

Two laser ablation sessions were performed with a dry and wet plasma (see Methods), with different tuning conditions between the two (Table 1). This was done to test whether the addition of water to the plasma would reduce or remove the background elevation around $m/z \approx 10$ observed during the ablation of Ca-rich bearing materials under the typical dry plasma conditions of LA-MC-ICPMS (although we note that our

solution mode experiments above show that Ca-bearing wet plasma conditions do also yield an elevated background). When ablating NIST SRM 612 under otherwise identical conditions (with a Milli-Q uptake rate of $100 \mu\text{L min}^{-1}$), the boron sensitivity was ~ 2.5 times higher in dry *versus* wet plasma conditions (3.2 and $1.2 \text{ mV per } \mu\text{g g}^{-1}$, respectively). The boron useful ion yield for the dry plasma was $2.47 \times 10^{-4} \pm 0.12 \times 10^{-4}$ (2 SD of the calculated useful ion yields through a session, for each NIST SRM 612 measurement), almost twice as high as that of the wet plasma ($1.35 \times 10^{-4} \pm 0.07 \times 10^{-4}$). Combined with the higher background of the wet plasma in this study, the signal-to-background ratio was much lower compared to a typical dry plasma session, ranging from ~ 2 (MACS-3; $[\text{B}] \approx 6 \mu\text{g g}^{-1}$) to ~ 14 (JCP-1, $[\text{B}] \approx 50 \mu\text{g g}^{-1}$) compared to the dry plasma with values ranging from ~ 64 (MACS-3) to ~ 575 (JCP-1).



Moreover, we find that (i) the magnitude of the scattered interference on $m/z \approx 10$ was proportionally similar to that of the dry plasma conditions when normalised to the sensitivity change (Fig. 2) and (ii) the relationship between the measured inaccuracy ($\Delta\delta^{11}\text{B}$) and the B/Ca of the standard (here measured as the ratio of the signal intensity of ^{11}B and the interference on $m/z = 10.035$) derived from three commonly utilised carbonate reference materials¹⁹ appears similar in both magnitude and trend, with the difference in the curvature of the regression likely originating from the different instrument tuning between dry and wet plasma conditions.

In conclusion, the addition of water to the plasma during laser ablation sampling does not appear to improve the precision or accuracy of boron isotope measurements, nor reduce or remove the scattered interference around $m/z \approx 10$. However, boron sensitivity is decreased to almost half of that in dry plasma conditions, which will impact data quality through its impact on counting statistics. Although adding water to the plasma during laser ablation has been shown to increase the precision of some elemental and isotopic measurements on ICPMS and MC-ICPMS and even reduce some interferences,^{40–44} this is not the case for the measurement of boron isotopes as experimentally determined here.

Evaluating the source of the elevated baseline using materials with different matrices. In order to evaluate the relative contribution of Ca and Mg (as the main cations in carbonates) to the elevated baseline centred around $m/z \approx 10$ during LA-MC-ICPMS measurements, thus extending previous work,^{17–19} we performed mass scans during ablation of magnesite, dolomite, and calcite (Fig. 3), using our typical conditions for spatially-resolved $\delta^{11}\text{B}$ LA-MC-ICPMS analysis of calcium carbonates (Table 1).

Ablation of calcite shows the highest elevated baseline signal ($\sim 390 \mu\text{V}$ on $m/z \approx 9.979$), while ablation of magnesite has the lowest of the materials investigated here ($\sim 200 \mu\text{V}$), compared to a typical blank measurement ($\sim 145 \mu\text{V}$). It is worth noting that the ablation of magnesite still displays a significant background elevation around $m/z \approx 10$ compared to the blank measurement. This would imply either that Ca is not the only ion responsible for the background elevation or that the magnesite contains minor Ca impurities. All three carbonates were characterised using FTIR and were found to have $\text{CO}_3 \nu_4$ vibration maxima close to published values in all cases (see Fig. S1†). Fietzke and Anagnostou (2023)²⁰ suggested that scattered Ar^+ ions are also responsible for the background elevation centred around $m/z \approx 10$, which could explain why a blank measurement has a background elevation at all in this region of interest and why baseline scans during ablation of magnesite are characterised by a higher background elevation compared to blank, since the $^{40}\text{Ar}^{4+}$ ion beam intensity is elevated compared to the blank measurement, and that the production of $^{40}\text{Ar}^{4+}$ and Ar^+ are both related. Based on this, the interference centred around $m/z \approx 10$ should be a function of both $[\text{Ca}]$ and scattered Ar^+ , here indirectly measured using the $^{40}\text{Ar}^{4+}$ ion beam intensity. When displaying the interference around $m/z \approx 10$ as a function of matrix $[\text{Ca}]$ alone, we find a significant linear relationship between the two, with $R^2 = 0.926$ and root mean square error (RMSE) $\approx 24 \mu\text{V}$ (Fig. S2a†). When regressing the interference against the measured $^{40}\text{Ar}^{4+}$ ion beam intensity alone, we find a less robust linear relationship with $R^2 = 0.834$ and RMSE $\approx 36 \mu\text{V}$ (Fig. S2b†). However, when combining both and multiplying the measured $^{40}\text{Ar}^{4+}$ ion beam by a unitless factor (optimised for maximum goodness of fit; Fig. S3†), we find a more robust linear relationship compared to $[\text{Ca}]$ alone,

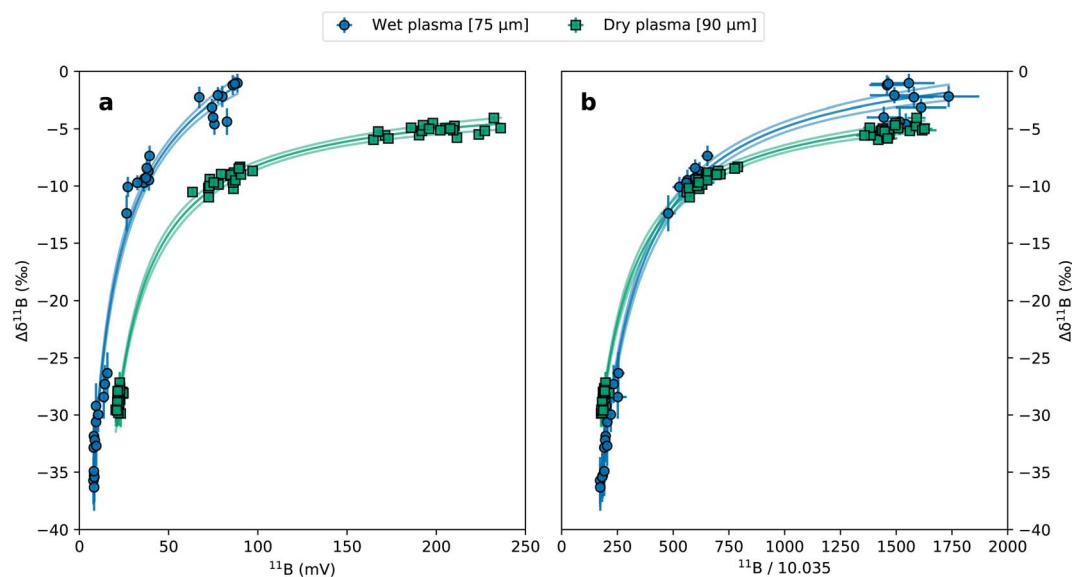


Fig. 2 Variation of the measured inaccuracy of LA boron isotope measurement ($\Delta\delta^{11}\text{B}$) of three carbonate standards (MACS-3, JCT-1, and JCP-1) in a dry and wet plasma setup. (a) $\Delta\delta^{11}\text{B}$ as a function of measured ^{11}B voltage both with (wet) and without (dry) Milli-Q aspirated into the ablation gas stream. (b) $\Delta\delta^{11}\text{B}$ as a function of the ratio between measured ^{11}B voltage and the measured Ca interference on mass 10.035. Note that the two sessions were carried out using different laser beam diameters, such that the dry plasma measurements are more precise than those performed with a wet plasma and spot size of 75 μm .



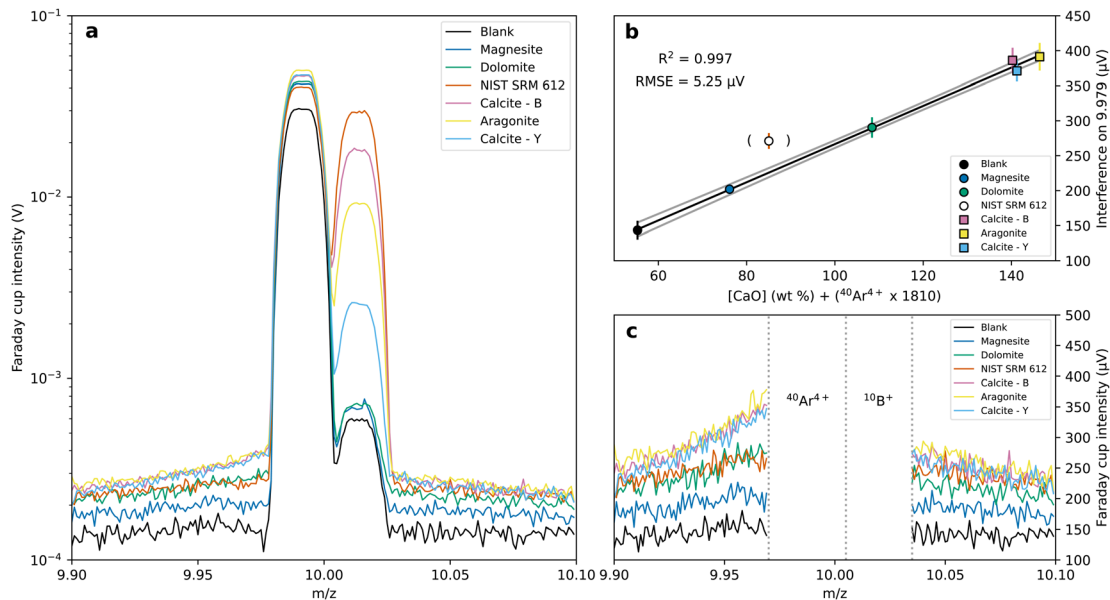


Fig. 3 Interference around $m/z \approx 10$ during the ablation of different matrices using LA-MC-ICPMS. (a) Mass scans in the region around ^{10}B ($m/z \approx 9.9$ to 10.1) during ablation of matrices with different Ca concentrations. The measurement was performed using a $10^{13} \Omega$ resistor with materials ablated using a $90 \mu\text{m}$ spot at 6 J cm^{-2} fluence and 10 Hz repetition rate. (b) Average background elevation at $m/z \approx 9.979$ as a function of matrix $[\text{CaO}]$ and $^{40}\text{Ar}^{4+}$ ion beam intensity multiplied by a unitless factor (see text). NIST SRM 612 was excluded from the linear fit, see Fig. S4† for a linear regression including all data. The displayed uncertainty is the 2 SE of the voltage between $m/z \approx 9.9$ and 9.98 . (c) Close-up of panel (a) in the region of the interference, excluding the peaks of $^{10}\text{B}^{+}$, to better distinguish the different sample matrices. Calcite-B and calcite-Y refer to the standards DE-B and DE-Y (in-house calcite standards).

with $R^2 = 0.969$ and $\text{RMSE} \approx 16 \mu\text{V}$ (Fig. S4†). NIST SRM 612 appears to have a higher measured interference compared to the derived linear regression between the interference and a combination of $[\text{Ca}]$ and $^{40}\text{Ar}^{4+}$ (Fig. 3b). This could be because the ionisation behaviour of NIST SRM 612-derived aerosols in the plasma differs from that of the carbonate, therefore yielding a lower $^{40}\text{Ar}^{4+}$ ion beam intensity (and thus scattered Ar^{+} in the flight tube) compared to the carbonate samples. Indeed, when regressing $[\text{Ca}]$ and $^{40}\text{Ar}^{4+}$ against the baseline elevation for the carbonate samples only, we find an even more robust linear relationship than before, with a $R^2 = 0.997$ and $\text{RMSE} \approx 5 \mu\text{V}$ (Fig. 3).

Since the baseline elevation centred on $m/z \approx 10$ during ablation of magnesite is more likely to originate from the increased inflow of Ar^{+} ions, this corroborates both the results from Fietzke and Anagnostou (2023),²⁰ and the results from our solution experiments (Fig. 1) where there is no measurable contribution of the Mg matrix to the background elevation around $m/z \approx 10$.

Inaccuracy of boron isotope analysis due to mass loading

Here we explore the possible effect of plasma mass loading by varying the laser spot size during the analysis of a geological calcite standard and relate this to the determined ablated masses (Fig. 4 and 5).

Ablation rate of various carbonate materials. To better understand the degree to which variable ablation rates between different materials might impact considerations surrounding plasma loading effects, we determined the ablation rates of

a range of common carbonate materials and standards as well as the NIST SRM 612 glass under variable fluences (Fig. 4). Measured ablation rates range from 180 nm per pulse (NIST SRM 612) to 380 nm per pulse (JCP-1 pressed pellet) at a laser fluence of $\sim 6 \text{ J cm}^{-2}$ (all measurements were performed with a $75 \mu\text{m}$ beam diameter). The substantially different ablation rates of the different standard pelleting approaches, *i.e.*, pressed powder (PP) *versus* nano-pellets (NP), and between both of these and intact samples, is shown in Fig. 4a. Grouping the standards together into these broad material types, it becomes apparent that the different preparation methodologies of the standards have a great impact on their ablation rates. Both solid carbonates and silicate glasses have a similar ablation rate with an average of $187 \pm 5 \text{ nm per pulse}$ (2 SD quadratically propagated uncertainty). In contrast, the NP standards have an average ablation rate of $260 \pm 13 \text{ nm per pulse}$ while the PP standards have an average ablation rate of $367 \pm 31 \text{ nm per pulse}$ (Fig. 4). The determining factors for the ablation rate of a solid sample by laser ablation are numerous and include: the wavelength of the laser,^{45,46} pulse width of the laser,^{47,48} the absorbance and reflectance of the material at the given laser wavelength,⁴⁹ and the energy density of the laser pulse at the sample surface.^{50,51} We decided to determine the ablation rate of the aforementioned standard groups as a function of laser fluence since it is the only parameter from the above list which can be changed through an analytical session (Fig. 4b). The relationship between ablation rate and laser fluence is closer to a power function, passing through the origin, although with an almost linear relationship between laser fluence and ablation



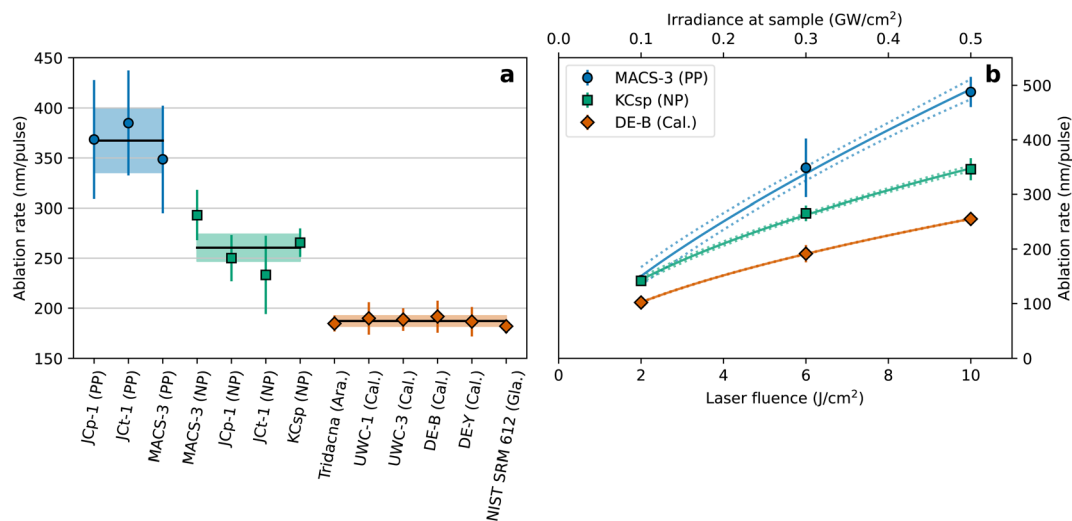


Fig. 4 Ablation rate of different carbonate materials routinely utilised or analysed for LA-MC-ICPMS $\delta^{11}\text{B}$ analysis. (a) Ablation rate in nm per pulse of different materials analysed using a RESOLUTION 193 nm ArF laser, fluence of $\sim 6 \text{ J cm}^{-2}$ and a $75 \mu\text{m}$ diameter circular laser beam (see Methods). The uncertainty is the 2 SD of the measured depth of 15 ablated craters. PP: pressed pellet, NP: nano pellet, Ara.: aragonite, Cal.: calcite, and Gla.: glass. The materials are grouped into three categories according to their broad characteristics, which coincides with their overall type, namely PP, NP, and intact; solid lines depict the mean of each of these with 2 SD variability displayed by the shaded region. (b) Ablation rate variations of three representative materials (namely MACS-3 – PP, KCsp – NP, and DE-B – Cal.) of the three aforementioned groups, using laser fluences ranging between 2–10 J cm^{-2} . KCsp is a speleothem-derived NP standard. A power function was fitted to the measured ablation rate, the dotted lines represent the 2 SD of the fit. For fluences greater than $\sim 2 \text{ J cm}^{-2}$, the ablation of the different materials displays an almost linear relationship with laser fluence. The data presented here can be found in Table S1.†

rate at fluences higher than 2 J cm^{-2} , as shown in previous experiments.⁵⁰ The ablation rate of the three groups differs in magnitude, but all share a similar trend. These ablation rates

are slightly higher than previously reported on the same model of laser ablation system (RESOLUTION M-50, ArF excimer) where an ablation rate of $83 \pm 1 \text{ nm}$ per pulse on aragonitic shell was

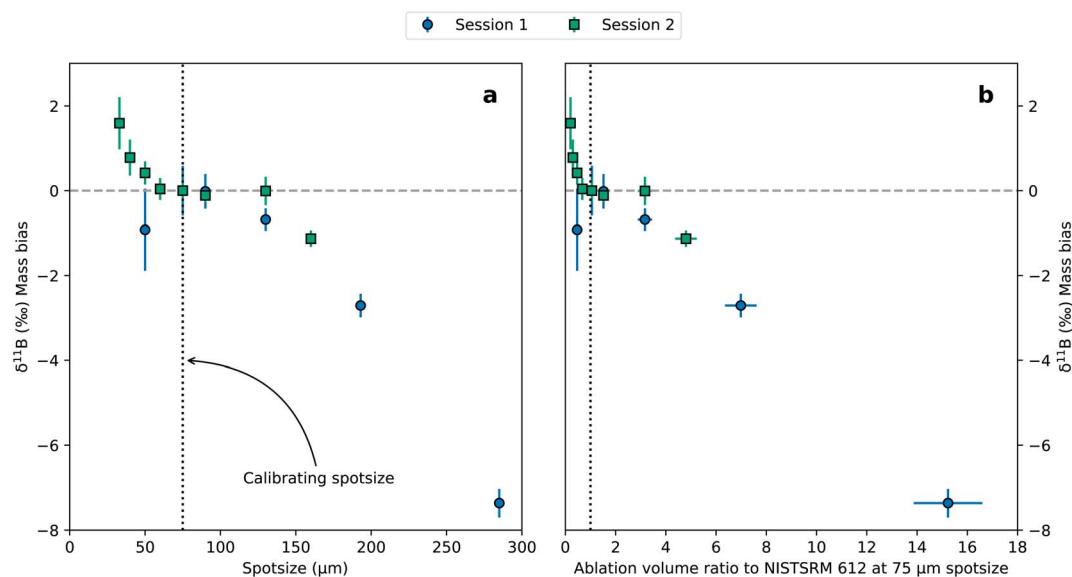


Fig. 5 Measured boron isotope inaccuracies of the in-house DE-B calcite standard during LA-MC-ICPMS analysis under different plasma loading scenarios across two analytical sessions. (a) Measured boron isotope mass bias as a function of laser beam diameter, standardised but performing the mass bias correction standard measurements using the same spot size in all cases (displayed as the vertical dotted line). The data were mass bias corrected using NIST SRM 612 as a calibrating standard ablated using a spot size of $75 \mu\text{m}$, 6 Hz laser repetition rate, and 6 J cm^{-2} laser fluence. The mass bias is calculated by subtracting the measurement of the DE-B calcite performed at the same spot size as the NIST SRM 612 from the measured $\delta^{11}\text{B}$ of DE-B at other laser spot sizes. (b) Measured boron isotope mass bias as a function of ablation volume ratio to NIST SRM 612. Error bars show the 2 SE of the 15 measurements for a given laser spot size, including the propagated uncertainty from the ablation of both the DE-B calcite and NIST SRM 612.



measured using an SEM when ablated using a fluence of $\sim 2.5 \text{ J cm}^{-2}$, although we note that aragonite is characterised by a slightly lower ablation rate than calcite, to which we compare here (in most cases, see Fig. 4).⁵²

The variable ablation rate of different materials can induce differences in the mass loading of the plasma, which may impact the measured ratio of boron isotopes. This can further influence measurement accuracy if the standards used to calibrate a measurement of a given sample have a different ablation rate. The different plasma loads can be achieved either by changing the laser spot size, laser repetition rate, or simply by measuring materials characterised by different ablation rates. The latter becomes difficult to take into account when choosing ablation conditions for an analytical session. For example, it is sometimes desirable to change ablation conditions (either laser spot size, repetition rate, or fluence) between standard and analytes to achieve signal matching between the two to prevent ion counters from overloading.²² In other cases, it is more important to maintain constant conditions when analysing standards and analytes such that no additional unconstrained fractionation occurs between samples of different concentrations.¹⁹ In this case, the laser spot size, repetition rate, and fluence are kept constant throughout an analytical session. During such a session, if the ablation rate of different samples/standards differs to a large degree, differential mass bias may occur between samples/standards with lower and higher ablation rates.

Mass loading-induced isotopic bias. To investigate possible plasma loading-induced analytical mass bias during laser ablation of calcium carbonate samples, we analysed the in-house standard DE-B (calcite) under a wide variety of spot sizes (33–285 μm ; this ~ 8 fold increase corresponds to an $\sim 75\times$ larger ablation area) across two different analytical sessions. To calibrate the analyses, *i.e.* to convert measured $^{11}\text{B}/^{10}\text{B}$ into $\delta^{11}\text{B}$, we measured NIST SRM 612 using a 75 μm spot size bracketed around the experiments and corrected for the B/Ca (m/z 11/10.035) following Standish *et al.* (2019)¹⁸ and Evans *et al.* (2021).¹⁹ Data from all spot sizes were calibrated to this carbonate standard regression line, as in the absence of any other factor, the B/Ca (11/10.035) ratio should be independent of the laser beam diameter. The resulting measured boron isotopic composition of DE-B under different plasma loading conditions are displayed in Fig. 5.

When the spot size on the analyte is bigger than the spot size on NIST SRM 612 used for calibration, we observe a decreasing trend in measured $\delta^{11}\text{B}$ (negative isotopic mass bias) as also previously reported in the case of silicates^{26,27} and carbonates.¹⁷ This negative mass bias increases exponentially with increasing spot size (Fig. 5a). When converting the laser spot size into relative ablation volume, we find that the mass bias trend is closer to a linear relationship than relative to spot size (Fig. 5b).

When the analyte spot size is smaller than the spot size used for the calibrating standard, we observe a steeper trend at spot sizes smaller than that of the calibration line, with bias increasing exponentially as the analyte spot size reduces. This trend could be explained either *via* (i) ablation pit geometry, with a greater influence of aspect ratio on down-hole

fractionation when using smaller laser beam diameters,⁵³ and/or (ii) a plasma loading effect on boron isotope measurements. Similarly, experimental data from Martin *et al.* (2015),²⁶ and Kimura *et al.* (2016)²⁷ demonstrated strong negative boron isotope biases when increasing the plasma loading during LA-MC-ICPMS analysis of silicates.

Varying laser spot size, fluence, and wavelength not only changes the mass load of the plasma but also the aerosol size distribution arriving into the plasma.^{54–58} This impacts the magnitude of the bias in isotopic measurements as the size of the aerosols entering the plasma impacts the ionisation efficiency within the plasma.⁵⁹ For instance, the longer the ionisation process takes (*i.e.* the larger the aerosol or the cooler the plasma) the greater the degree of the resulting mass bias.^{60,61} Physical modelling studies have shown that an increase in plasma mass loading leads to a shift in the temperature and plasma electron density profile, impacting where the atoms are ionised.⁶² This is corroborated by the isotopic model of Fietzke and Anagnostou (2023)²⁰ in which an increase in plasma loading shifts the position in the plasma at which boron is released from the aerosols and thus its measured intensity and isotopic signature.

Since we deduced that the difference in ablation rate between the pressed-pellet (PP) and intact calcite standards is almost two fold (Fig. 4), and that a measured isotopic mass bias can arise when the plasma loading differs between the analysis of calibrating standards and analytes, we can estimate the greatest difference in ablated volume between different types of analyte and their potential associated boron isotopic mass bias. If, during a sequence, all standards are ablated with a 75 μm spot size and under typical laser ablation parameters for the FIERCE laboratory (fluence = 6 J cm^{-2} , repetition rate = 6 Hz, analysis duration = 60 s), the calibrating standard NIST SRM 612 would ablate $2.61 \times 10^5 \pm 0.09 \times 10^5 \mu\text{m}^3$ of material while a pressed pellet would ablate $5.29 \times 10^5 \pm 0.85 \times 10^5 \mu\text{m}^3$, giving an ablation ratio between the two of 2.03 ± 0.33 (propagated 2 SD). Using the measured boron isotope bias during plasma loading above that of the calibrating standard (Fig. 5b), we can deduce a linear relationship between measured mass bias and the ratio between the calibrating standard ablated volume (here NIST SRM 612) and the analyte ablated volume (here JcP-1-PP). The linear relationship includes the measurements of boron isotope mass bias between spot sizes of 75 μm up to 285 μm , or between a standard/analyte ablation ratio between 1 and ~ 15 . We note that it is not strictly a linear relationship (Fig. 5b), but approximate it as such across a narrower range of ablation volumes than fully displayed in Fig. 5. Using this approximation, we can estimate that the expected boron isotope bias due to a difference in plasma loading between the calibrating standard and analyte with an ablation volume ratio of around 2.03 ± 0.33 to be approximately $-0.27\text{‰} \pm 0.22\text{‰}$. Although this estimate is not quantitative and can vary under different machine tunings, this magnitude of bias is not resolvable on either the scale of single spot laser analyses using the methodology of Evans *et al.* 2021 (ref. 19) and Standish *et al.* 2019 (ref. 18) ($\sim 0.5\text{‰}$ precision, 2 SD) or long-term reproducibility ($\sim 0.9\text{‰}$, 2 SD). This sub-permil bias is comparatively



smaller than the isotopic bias induced by the Ca^+ and Ar^+ baseline elevation around $m/z \approx 10$, as detailed in the previous sections, with biases from permil-level to several tens of permil (see Fig. 2). We would thus advise to prioritise matching the matrices of the calibration standards and analytes over matching their respective ablation rates.

The boron isotope bias induced by a difference in mass loading between the instrumental bias calibrating standard and analyte is not significant enough to be resolved with available analytical instrumentation for LA-MC-ICPMS on a single spot analysis. This means that the pressed- and nano-pellet sample preparation methods for carbonate materials, in spite of their higher ablation rates, are well suited for *in situ* boron isotope measurement by LA-MC-ICPMS. However, this effect may be reflected in the long-term accuracy of the methodology, for example, this could explain $\sim 30\%$ of the observed minor inaccuracy ($\sim 0.89\%$) in LA-MC-ICPMS $\delta^{11}\text{B}$ measurements in our laboratory,³³ and will potentially be relevant in the future with improvements in instrument precision.

Conclusions

The utility of precise spatially resolved measurements of boron isotopes in calcium carbonate samples has pushed the need for a better understanding of the different interferences and biases that may arise during LA-MC-ICPMS measurements to increase accuracy and reliability. *Via* the analysis of B-solutions with different matrices, we demonstrate that not only is the previously reported elevated baseline centred around $m/z \approx 10$ present during solution measurements of Ca-containing solutions under both dry and wet plasma conditions, but also that it is absent during analysis of Mg-containing solutions. This also underscores the importance of purification of boron from calcium carbonate sample matrices during solution measurements of boron isotopes. By performing laser-ablation analysis of Ca-rich and Ca-poor materials, we further corroborate that while Ca is the main contributor to the previously reported background elevation around $m/z \approx 10$, Ar^+ also contributes to an important component of this baseline signal. A combination of $[\text{Ca}]$ and $^{40}\text{Ar}^{4+}$ ion beam intensity (a proxy for Ar^+) best describes the measured interference across different sample matrices.

In addition, we examine the extent to which the typically used, high sensitivity, yet less robust, plasma tuning for LA-MC-ICPMS boron isotope measurements is sensitive to plasma loading effects. Understanding this issue is crucial when calibrating the instrumental bias at a different plasma load compared to that of the analytes, due to differences in material type. Through ablation rate measurements, we estimated that, although likely to be small for most calibration approaches, the boron isotope mass bias induced by a difference in ablation rate between solid standards and pressed pellets of carbonate samples might be problematic, especially in future when instrumental developments improve the precision for boron isotope measurements. This boron isotope mass bias induced by plasma mass loading has been previously reported for boron isotope measurements on other LA-MC-ICPMS instrument

combinations as well as other sample matrices (*i.e.* silicates).¹⁹ This highlights the need for careful consideration of plasma loading when measuring boron isotopes using LA-MC-ICPMS, regardless of the analyte matrix or instrument.

Data availability

The data supporting this article have been included as part of the ESI.†

Author contributions

Douglas Coenen: conceptualization, methodology, software, formal analysis, investigation, data curation, writing – original draft, visualization. David Evans: conceptualization, methodology, validation, investigation, resources, writing – review and editing, supervision, project administration, funding acquisition. Hana Jurikova: methodology, investigation, writing – review and editing. Matthew Dumont: methodology, investigation, writing – review and editing. James Rae: writing – review and editing, funding acquisition. Wolfgang Müller: conceptualization, writing – review and editing, supervision, project administration, funding acquisition.

Conflicts of interest

There are no conflicts to declare.

Acknowledgements

We thank Alexander Schmidt and Linda Marko for their help with solution and LA-MC-ICPMS analysis and Dieter Garbe-Schönberg for providing the KCSp standard. FIERCE is financially supported by the Wilhelm and Else Heraeus Foundation and by the Deutsche Forschungsgemeinschaft (DFG: INST 161/921-1 FUGG, INST 161/923-1 FUGG and INST 161/1073-1 FUGG), which is gratefully acknowledged. This research was funded through the VeWA consortium by the LOEWE programme of the Hessen Ministry of Higher Education, Research and the Arts, Germany. James Rae, Hana Jurikova, and Matthew Dumont acknowledge funding from the Royal Society of Edinburgh (RSE Saltire International Collaboration, grant number 1964), and Hana Jurikova also thanks the Leverhulme Trust Early Career Fellowship for funding (ECF-2023-199). We would like to thank the editor and the two anonymous reviewers for taking the time and effort necessary to review the manuscript. We sincerely appreciate all of the valuable comments and suggestions they provided, which resulted in an improved version of the manuscript. This is FIERCE contribution No. 171.

Notes and references

- 1 H. Marschall and G. Foster, Boron isotopes: the fifth element, *Advances in Isotope Geochemistry*, Springer, 2018.
- 2 M. R. Palmer, *Geology*, 1991, **19**, 215.
- 3 H. R. Marschall, in *Boron Isotopes: the Fifth Element*, ed. H. Marschall and G. Foster, Springer, 2018, pp. 189–215.



- 4 J. W. B. Rae, Y. G. Zhang, X. Liu, G. L. Foster, H. M. Stoll and R. D. M. Whiteford, *Annu. Rev. Earth Planet. Sci.*, 2021, **49**, 599–631.
- 5 M. T. McCulloch, J. P. D'Olivo, J. Falter, M. Holcomb and J. A. Trotter, *Nat. Commun.*, 2017, **8**, 15686.
- 6 A. C. Gagnon, A. M. Gothmann, O. Branson, J. W. B. Rae and J. A. Stewart, *Earth Planet. Sci. Lett.*, 2021, **554**, 116662.
- 7 G. L. Foster, B. Hönisch, G. Paris, G. S. Dwyer, J. W. B. Rae, T. Elliott, J. Gaillardet, N. G. Hemming, P. Louvat and A. Vengosh, *Chem. Geol.*, 2013, **378**, 1–14.
- 8 M. T. McCulloch, M. Holcomb, K. Rankenburg and J. A. Trotter, *Rapid Commun. Mass Spectrom.*, 2014, **28**, 2704–2712.
- 9 X. Chen, F. Teng and D. C. Catling, *Rapid Commun. Mass Spectrom.*, 2019, **33**, 1169–1178.
- 10 M.-y. He, Y.-k. Xiao, Z.-d. Jin, Y.-q. Ma, J. Xiao, Y.-l. Zhang, C.-g. Luo and F. Zhang, *Anal. Chem.*, 2013, **85**, 6248–6253.
- 11 M. Trudgill, S. Nuber, H. E. Block, J. Crumpton-Banks, H. Jurikova, E. Littley, M. Shankle, C. Xu, R. C. J. Steele and J. W. B. Rae, *Geochem., Geophys., Geosyst.*, 2024, **25**, e2023GC011350.
- 12 C. Rollion-Bard and J. Erez, *Geochim. Cosmochim. Acta*, 2010, **74**, 1530–1536.
- 13 H. Jurikova, V. Liebetrau, J. Raddatz, J. Fietzke, J. Trotter, A. Rocholl, S. Krause, M. McCulloch, A. Rüggeberg and A. Eisenhauer, *Chem. Geol.*, 2019, **513**, 143–152.
- 14 P. Le Roux, S. Shirey, L. Benton, E. Hauri and T. Mock, *Chem. Geol.*, 2004, **203**, 123–138.
- 15 J. Fietzke, A. Heinemann, I. Taubner, F. Böhm, J. Erez and A. Eisenhauer, *J. Anal. At. Spectrom.*, 2010, **25**, 1953.
- 16 F. Thil, D. Blamart, C. Assailly, C. E. Lazareth, T. Leblanc, J. Butsher and E. Douville, *Rapid Commun. Mass Spectrom.*, 2016, **30**, 359–371.
- 17 A. Sadekov, N. S. Lloyd, S. Misra, J. Trotter, J. D'Olivo and M. McCulloch, *J. Anal. At. Spectrom.*, 2019, **34**, 550–560.
- 18 C. D. Standish, T. B. Chalk, T. L. Babila, J. A. Milton, M. R. Palmer and G. L. Foster, *Rapid Commun. Mass Spectrom.*, 2019, **33**, 959–968.
- 19 D. Evans, A. Gerdes, D. Coenen, H. R. Marschall and W. Müller, *J. Anal. At. Spectrom.*, 2021, **36**, 1607–1617.
- 20 J. Fietzke and E. Anagnostou, *Geostand. Geoanal. Res.*, 2023, **47**, 481–492.
- 21 M. Raitzsch, C. Rollion-Bard, I. Horn, G. Steinhoefel, A. Benthien, K.-U. Richter, M. Buisson, P. Louvat and J. Bijma, *Biogeosciences*, 2020, **17**, 5365–5375.
- 22 G. Steinhoefel, K. K. Beck, A. Benthien, K. Richter, G. M. Schmidt-Grieb and J. Bijma, *Rapid Commun. Mass Spectrom.*, 2023, **37**, e9508.
- 23 D. Mayk, J. Fietzke, E. Anagnostou and A. Paytan, *Chem. Geol.*, 2020, **531**, 119351.
- 24 J. Fietzke and M. Wall, *Sci. Adv.*, 2022, **8**, eabj4172.
- 25 N. S. Lloyd, A. Y. Sadekov and S. Misra, *Rapid Commun. Mass Spectrom.*, 2017, **32**, 9–18.
- 26 C. Martin, E. Ponzevera and G. Harlow, *Chem. Geol.*, 2015, **412**, 107–116.
- 27 J.-I. Kimura, Q. Chang, T. Ishikawa and T. Tsujimori, *J. Anal. At. Spectrom.*, 2016, **31**, 2305–2320.
- 28 D. Evans and W. Müller, *Geostand. Geoanal. Res.*, 2018, **42**, 159–188.
- 29 L. Lin, Z. Hu, L. Yang, W. Zhang, Y. Liu, S. Gao and S. Hu, *Chem. Geol.*, 2014, **386**, 22–30.
- 30 J. Fietzke and M. Frische, *J. Anal. At. Spectrom.*, 2016, **31**, 234–244.
- 31 M. Gutjahr, L. Bordier, E. Douville, J. Farmer, G. L. Foster, E. C. Hathorne, B. Hönisch, D. Lemarchand, P. Louvat, M. McCulloch, J. Noireaux, N. Pallavicini, J. W. B. Rae, I. Rodushkin, P. Roux, J. A. Stewart, F. Thil and C.-F. You, *Geostand. Geoanal. Res.*, 2020, **45**, 59–75.
- 32 S. Wilson, A. Koenig and R. Orklid, *Geochim. Cosmochim. Acta, Suppl.*, 2008, **72**, A1025.
- 33 D. Coenen, D. Evans, H. Hauzer, R. Nambiar, H. Jurikova, M. Dumont, P. Kanna, J. Rae, J. Erez, L. Cotton, W. Renema and W. Müller, *Geochim. Cosmochim. Acta*, 2024, **378**, 217–233.
- 34 C. M. Graham, J. W. Valley, J. M. Eiler and H. Wada, *Contrib. Mineral. Petrol.*, 1998, **132**, 371–389.
- 35 S. M. Eggins, L. P. J. Kinsley and J. M. G. Shelley, *Appl. Surf. Sci.*, 1998, 278–286.
- 36 W. Müller, M. Shelley, P. Miller and S. Broude, *J. Anal. At. Spectrom.*, 2009, **24**, 209–214.
- 37 P. K. Diwakar, J. J. Gonzalez, S. S. Harilal, R. E. Russo and A. Hassanein, *J. Anal. At. Spectrom.*, 2014, **29**, 339–346.
- 38 G. L. Foster, *Earth Planet. Sci. Lett.*, 2008, **271**, 254–266.
- 39 J. Barling and D. Weis, *J. Anal. At. Spectrom.*, 2008, **23**, 1017.
- 40 J. Lin, Y. Liu, A. Yang, W. Chen, L. Zhu and Z. Hu, *J. Anal. At. Spectrom.*, 2022, **37**, 592–602.
- 41 J. Lu, W. Chen, J. Sun, J. Lin, T. Luo, Y.-H. Liu, K.-D. Zhao, S.-Y. Jiang and Y.-S. Liu, *J. Anal. At. Spectrom.*, 2022, **37**, 1665–1674.
- 42 X. Tan, J. Koch, D. Günther and B. Hattendorf, *Geostand. Geoanal. Res.*, 2023, 12538.
- 43 C. O'Connor, B. L. Sharp and P. Evans, *J. Anal. At. Spectrom.*, 2006, **21**, 556.
- 44 M. Schönbächler, R. W. Carlson, M. F. Horan, T. D. Mock and E. H. Hauri, *Int. J. Mass Spectrom.*, 2007, **261**, 183–191.
- 45 I. Horn, M. Guillong and D. Günther, *Appl. Surf. Sci.*, 2001, **182**, 91–102.
- 46 J. Gonzalez, X. L. Mao, J. Roy, S. S. Mao and R. E. Russo, *J. Anal. At. Spectrom.*, 2002, **17**, 1108–1113.
- 47 R. Stoian, D. Ashkenasi, A. Rosenfeld and E. E. B. Campbell, *Phys. Rev. B*, 2000, **62**, 13167–13173.
- 48 K. Jenkins, K. Goemann, I. Belousov, M. Morissette and L. Danyushevsky, *Geostand. Geoanal. Res.*, 2023, **47**, 267–295.
- 49 W. Müller and J. Fietzke, *Elements*, 2016, **12**, 329–334.
- 50 J. Byskov-Nielsen, J.-M. Savolainen, M. S. Christensen and P. Balling, *Appl. Phys. A: Mater. Sci. Process.*, 2010, **101**, 97–101.
- 51 M. E. Shaheen and B. J. Fryer, *Laser Part. Beams*, 2012, **30**, 473–479.
- 52 N. Griffiths, W. Müller, K. G. Johnson and O. A. Aguilera, *Palaeogeogr., Palaeoclimatol., Palaeoecol.*, 2013, **369**, 185–200.
- 53 I. Horn, R. L. Rudnick and W. F. McDonough, *Chem. Geol.*, 2000, **164**, 281–301.



- 54 M. L. Alexander, M. R. Smith, J. S. Hartman, A. Mendoza and D. W. Koppenaal, *Appl. Surf. Sci.*, 1998, **127–129**, 255–261.
- 55 H.-R. Kuhn, J. Koch, R. Hergenröder, K. Niemax, M. Kalberer and D. Günther, *J. Anal. At. Spectrom.*, 2005, **20**, 894.
- 56 B. K. Kuhn, K. Birbaum, Y. Luo and D. Günther, *J. Anal. At. Spectrom.*, 2010, **25**, 21–27.
- 57 H.-R. Kuhn and D. Günther, *J. Anal. At. Spectrom.*, 2006, **21**, 1209–1213.
- 58 I. Krosiakova and D. Günther, *J. Anal. At. Spectrom.*, 2007, **22**, 51–62.
- 59 J. Fuchs, M. Aghaei, T. D. Schachel, M. Sperling, A. Bogaerts and U. Karst, *Anal. Chem.*, 2018, **90**, 10271–10278.
- 60 H.-R. Kuhn, M. Guillong and D. Günther, *Anal. Bioanal. Chem.*, 2004, **378**, 1069–1074.
- 61 I. Horn and F. Von Blanckenburg, *Spectrochim. Acta, Part B*, 2007, **62**, 410–422.
- 62 M. Aghaei, H. Lindner and A. Bogaerts, *Anal. Chem.*, 2016, **88**, 8005–8018.

